Pattern Formation in Traffic

Martine Barons

Centre for Complexity Science, Zeeman Building, University of Warwick, Coventry CV4 7AL

Abstract

Traffic flow can be modelled as a density of microscopic particles like a fluid, or as individual cars with drivers making decisions based on the information they have. The aim of this study was to further the understanding of the connection between these two descriptions by comparing traffic flow described by a scalar conservation law model and by a cellular automata model. The simulations based on cellular automata support the conclusion that the corresponding conservation law describes the large scale microscopic description correctly using just standard entropy conditions. This discovery was partly unexpected.
The cellular automata model was induced to produce stable stop and go wave behaviour over a many-run aggregation, and an attempt was made to scale this up to physically realistic spatiotemporal size.
This simple cellular automata model showed stationary patterns producing spatially separate high and low density phases which existed in all sizes and for which no typical size can be identified, in correspondence with observations of real traffic flow.

1. Introduction

The flow of road traffic can be modelled on a microscopic level, for example by cellular automata, and on a macroscopic level by partial differential equations (PDE). There is not full agreement between these two description, particularly in the fact that simple Markov chain models are capable of predicting all the basic space-time patterns of real traffic whilst the macroscopic models are not. A simple Markov model is used to demonstrate the successes and limits of reproducing physically realistic traffic behaviour with a microscopic model. The connection with the macroscopic model described by the classic Lighthill, Whitham and Richards (LWR) PDE model is shown through the analysis of the flux / density diagram, called the Fundamental Diagram. Data samples from the M42 motorway are used to compare with the output of both models to assess their accuracy in predicting the behaviour of real traffic.

In the 1950s James Lighthill and Gerald Whitham, two experts in fluid dynamics, (and independently P. Richards) thought that the Navier-Stokes equations describing the flow of water could be used to describe the flow of vehicular traffic [1]. The Navier-Stokes equations are a set of partial differential equations expressing conservation of mass, momentum and energy. Treating vehicles as small particles and their density as the main quantity to be considered, the assumption is made that the number of cars is conserved, making this a conservation law [12]. Since traffic jams display sharp discontinuities, there is a correspondence between traffic jams and shock waves[5, 7]. As solutions to fluid dynamic models can develop discontinuities in finite time, even starting from smooth initial data, such models for traffic flow seem appropriate [2].
This conservation law is well described by an extensive and mature PDE theory which includes consideration of characteristics of the equation[9], weak solutions and admissibility criteria [2, 6, 8]. Cellular automata models are similarly well studied in many applications, and special cases have been identified [11, 13]. In relation to traffic, they have been used with various rules for driver behaviour [3, 10]. None of the approaches taken so far has been entirely satisfactory in predicting real traffic, particularly spatiotemporal patterns like stop and go waves, and there is some disagreement within the traffic modelling community as to the best approach. See [3] for a nice introduction.
The purpose of this study is to identify whether the Lighthill, Whitham and Richards PDE model can be made to predict the behaviour of the microscopic cellular automata model, whether new entropy conditions are needed, and if there is any relation between these and observed real data [4].
The following section gives an overview of the microscopic and macroscopic models, after which comes an exposition

of the simulation behaviour. The following section contains comparisons with real data and then conclusions are drawn.

2. Background on Traffic Modelling

2.1. Microscopic Model

The vehicles are modelled, using a Markov Chain representation, as particles on a one-dimensional lattice with periodic boundary conditions, where the probability of jumping to the next space depends only on the current configuration, and not on the jump history. The particle system has rates in figure 1

Figure 1: Jump rates for the microscopic model.
The simulation picks a site at random and, by considering it to be the second site from the left, determines if any of these four scenarios are matched. In addition to the rates, the initial density of cars can be varied. The 'cars' are initially distributed randomly on the sites of the one dimensional lattice $\Lambda_L[1 \dots L]$, $x \in \{0,1\}^{\Lambda_L}$ with periodic boundary conditions, to mimic a ring road and implement the conservation vehicles.

Continuous time dynamics are implemented via random sequential updating as follows: For configurations η and spatial locations x pick a site at random, uniformly from the entire lattice. If at site x , where the driver is, and $x+1$, the space in front, configuration $\eta(x) = 1$ and $\eta(x+1) = 0$, then generate a random number $\in [0,1]$. If this random number is less than the local rate, r depending on the values of $\eta(x-1)$ and $\eta(x+2)$ (r=1, α, β or γ), then $\eta(x)$ becomes 0 and $\eta(x+1)$ becomes 1. This replicates a car moving from its present location to the space in front.
The rates $C(\eta, \eta')$ are non zero only on the cases give in figure 1, written:

$$\begin{aligned} C(x, x+1, \eta) \quad = \quad & (1-\eta_{x-1})\eta_x(1-\eta_{x+1})(1-\eta_{x+2}) \; + \; \alpha\eta_{x-1}\eta_x(1-\eta_{x+1})\eta_{x+2} \\ & +\beta(1-\eta_{x-1})\eta_x(1-\eta_{x+1})\eta_{x+2} \; + \; \gamma\eta_{x-1}\eta_x(1-\eta_{x+1})(1-\eta_{x+2}) \end{aligned} \tag{1}$$

The Master Equation gives the probability, $\mathbb{P}_t(\eta)$ of being in configuration η as it changes over time t, as the probability of entering configuration η per unit time less the probability of leaving configuration η per unit time. Formally:

$$\frac{d}{dt}\mathbb{P}_t(\eta) = \sum_{\eta' \in x} C(\eta', \eta)\mathbb{P}_t(\eta') \; - \; \mathbb{P}_t(\eta) \sum_{\eta' \in x} C(\eta, \eta') \tag{2}$$

The ergodic theorem states that a finite state, irreducible Markov chain with finite state space is ergodic, so there exists a unique stationary distribution for every given number of cars, N, and density $\rho = \frac{N}{L}$, where L is the lattice size, and allows us to define the stationary current as:

$$j(\rho) = \mathbb{E}(C, (x, x+1, \eta)). \tag{3}$$

There is a special case of this kind of particle model, called the KLS model (Katz, Lebowitz, Spohn), with next nearest neighbour interactions, which is exactly solvable for periodic boundary conditions [11, 13]. It has parameters δ and $\epsilon \in (-1, 1)$ and its jump rates, relative to figure 1 are: $(1+\delta)$ corresponds to 1, $(1-\delta)$ corresponds to α, $(1-\epsilon)$ corresponds to β and $(1+\epsilon)$ corresponds to γ. Setting $\delta = \epsilon = 0.9$ and $(1+\delta) = 1$ gives $\alpha = \beta = \frac{1}{19}$, $\gamma = 1$.

2.2. Macroscopic Model

The Lighthill, Whitham and Richards model [1] is a PDE model describing the vehilces as particles and condsidering their density as the quantity of interest under the assumption of conservation of vehicles.

$$\frac{\partial}{\partial t}\rho(x,t) + \frac{\partial}{\partial x}j(\rho(x,t)) = 0 \tag{4}$$

where $\rho(x,t)$ is the density of cars with $\rho \in [0, \rho_{max}]$, $(x,t) \in \mathbb{R}^2$ and ρ_{max} is the maximum possible density of cars on the road. The flux is j and is defined as the number of vehicles passing a point in a given time interval. It may be written $j = \rho v$ with v the average velocity of vehicles. It is commonly assumed that v is a function of ρ only, so $j = j(\rho)$, the flux function. This assumption is adopted here. The law giving the flux as a function of the density is called the Fundamental Diagram, and is typically a non-linear, concave function. At small values of ρ, $j(\rho)$ is linear, but as density increases, the flux begins to decrease again. In real traffic this is the minimum safe braking distance reached when roads become crowded, and in a particle system may be thought of as repulsion between particles. Flux may also be denoted flow or current.
The standard fact for a nonlinear system like this is that classical solutions may not exist for some positive time, even if the initial datum is smooth. This can be shown by the method of characteristics.
A curve $t \to x(t)$ is a *characteristic* of this equation if

$$\frac{d}{dt}\rho(x(t),t) = 0 \;\forall\; t > 0. \tag{5}$$

Now by the chain rule,

$$\frac{d}{dt}\rho(x(t),t) = \frac{\partial}{\partial x}\rho(x(t),t)\frac{d}{dt}(x(t)) + \frac{\partial}{\partial t}\rho(x(t),t) = 0$$

and

$$\frac{\partial}{\partial x}j(\rho(x,t)) = j'(\rho(x,t))\frac{\partial}{\partial x}\rho(x,t)$$

From the PDE we know that

$$\frac{\partial}{\partial t}\rho(x(t),t) = -\frac{\partial}{\partial x}j(\rho(x(t),t)) = -j'(\rho(x(t),t)\frac{\partial}{\partial x}\rho(x(t),t)$$

Factorising gives

$$\frac{\partial}{\partial x}\rho(x(t),t)\left[\frac{\partial}{\partial t}x(t) - j'(\rho(x(t),t))\right] = 0$$

The first element of the product is zero if $\frac{\partial}{\partial x}(\rho(x,0)) = 0$, i.e if $\rho(x(0),0)$ is constant, but this is the trivial case.
The second element of the product is zero if

$$\frac{\partial}{\partial t}x(t) = j'(\rho(x(t),t)) = j'(\rho(x(0),0)$$

So characteristic curves are straight lines from each point, $(x,0)$, travelling with speed $\rho(x,0)$, and if $\rho(x,0)$ is differentiable, then the lines cover a slab $0 \le t \le T$ in a one to one fashion and these provide a solution to the Cauchy (initial value) problem.
When $\rho(x,0)$ is an increasing, smooth function of x, the straight lines cover the whole of the half plane x,t (where $t \ge 0$), in a one to one fashion, and this is a strong solution. But in the case that $\rho(x_1,0) \ge \rho(x_2,0)$ for some pair $x_1,\ x_2$, where $x_1 < x_2$, then the characteristics issuing from x_1 and x_2 intersect at time

$$t_c = \frac{(x_2 - x_1)}{j'(\rho(x_1,0)) - j'(\rho(x_2,0))} \tag{6}$$

At the point of intersection, $\rho(x,t_c)$ would have to be equal to both $\rho(x_1,0)$ and $\rho(x_2,0)$, an impossibility. So there is no continuous solution beyond the time t_c[5]. Thus the Lighthill, Whitham and Richards model is found to be inadequate

in that it produces multiple solutions where vehicles move into zones of greater congestion [6].
Riemann showed that solutions can be continued beyond the time when singularities form, as solutions in the integral sense. He also derived the law of propagation of discontinuities of solutions in the integral sense. These are weak solutions. It can be shown that within the class of solutions in the integrals sense, an initial value problem may have several solutions. Therefore, this class has to be narrowed. Principles for singling out admissible weak solutions are often referred to as entropy conditions, alluding to the classical gas dynamical prototype from which they first arose [7]. In that context, the second law of thermodynamics requires that the entropy production rate in all thermo-mechanical processes undergone by the gas must be non-negative: order or information cannot be produced. Since discontinuous solutions are introduced because of the collision of characteristics, only discontinuities which separate two characteristics which otherwise would impinge on each other are accepted, i.e. where

$$j'(\rho_L) \geq s \geq j'(\rho_R) \tag{7}$$

and s is the speed of propagation of the discontinuity, $j'(\rho_L)$ and $j'(\rho_R)$ are speeds $\rho(x, 0)$ of the characteristic curves to the left and right of the discontinuity. The speed s is given by the secant in the Fundamental Diagram

$$s = \frac{j(\rho_R) \; - \; j(\rho_L)}{\rho_R \; - \rho_L} \tag{8}$$

There is a well developed theory for admissibility of weak solutions depending on the convexity or concavity of the flux function [5]. It will be explained in section 3.2 when applied to the traffic model [9]

In the case that a PDE describes a physical system, such as the case of the Lighthill, Whitham and Richards model, then the admissibility criteria have also to select the solution that is right for the physical circumstances that give rise to it [7, 12]. Despite the fact that the Lighthill, Whitham and Richards model uses only the local flow density, whilst real drivers observe the traffic behind and ahead increasing their information, (7) may be interpreted physically in the case of concave flux functions as the *driver's ride impulse*: drivers approaching a jam do not stop until they reach the jam, and increase the traffic density at that point, but drivers leaving a jam move to less dense traffic, smoothing the discontinuity as at traffic lights [8]. These problems are often formulated as Riemann problems, which are initial value (Cauchy) problems with Heaviside initial data [2], such as

$$\rho(x, 0) = \begin{cases} \rho_L, & \text{for } x \leq 0 \\ \rho_R, & \text{for } x > 0 \end{cases}$$

For flux functions that are neither convex nor concave, e.g. figure 6, the Oleinik generalised entropy condition:

$$\frac{j(\rho) - j(\rho_L)}{\rho - \rho_L} \geq s \geq \frac{j(\rho) - j(\rho_R)}{\rho - \rho_R} \; \forall \rho \in [\rho_L, \rho_R] \tag{9}$$

guarantees a unique weak solution [9, 5]. For Riemann data lying in the concave regime of the flux function, (9) reduces to

$$\rho_L \leq \rho_R, \tag{10}$$

and in the convex regime to the opposite condition,

$$\rho_L \geq \rho_R. \tag{11}$$

Denoting the value of ρ for which the flux function changes from concave to convex as ρ_{cc} the entropy solutions satisfy the drivers ride impulse for Riemann problems with data $\rho_l, \rho_R \leq \rho_{cc}$. However for $\rho_l, \rho_R > \rho_{cc}$, the traffic flow reality is contradicted: drivers move into denser traffic smoothing the discontinuity (rarefaction), and into less dense traffic by a discontinuous shock wave. Gasser proposes an alternative, non-entropy solution

$$\begin{cases} if \; \rho_L < \rho_R, & \text{use the pure shock solution} \\ if \; \rho_L > \rho_R, & \text{use the Oleinik-admissible solution} \end{cases}$$

(9) and demonstrates that a stop and go wave structure would be preserved under this condition [9].
Knowles proposes admissibility based on Lax and Oleinik criteria and adds an entropy density which is strictly concave and shows that with this in force there are shocks admissible that fail to be admissible by the Lax or Oleinik criteria alone. However, the Gasser example of the stop and go wave cannot be replicated with this entropy density in force and concludes that there is a need to find admissibility condition based on traffic modelling, rather than on another discipline [7].

Gasser finds fault with the entropy solution method for the Lighthill, Whitham and Richards on the basis that realistic equilibrium flux functions are not concave, but consist of a concave part in the lower density regime and a convex part in the upper density regime as in figure 10. In the concave or convex case, the entropy solutions of Riemann problems consist of a single rarefaction or a single shock wave, in the nonconcave and nonconvex case they are in general combinations of rarefaction and shock waves. He further argues that in real traffic drivers' decisions are made based on more than local information as is the case in the model, i.e. information increases.

3. Theoretical results

3.1. Stationary Patterns

The Markov chain-based simulation is used to produce the desired space-time patterns seen in traffic, supported and verified with reference to the M42 data, and the theory of characteristics.
At the microscopic level a simple cellular automata simulation is used to produce all the basic space-time patterns such as free flow, congestion and stop and go waves. The traffic patterns are produced with this model by varying the rates α, β, γ defined above in figure 1. The physically corresponding system does not suggest absolute values for the rates, but suggests relationships between them. For example, a driver (at location x, the second lattice site from the left in figure 1) with clear road ahead (i.e 1 and γ) will move off more quickly than one moving towards more traffic (α and β) . In discrete time, those with a vehicle behind correspond to those who did not move during the last update, so represent starting from stationary. When these rates are small, this is a slow to start model. The main effects of the slow-to-start rules are a (small) reduction of the flow and a shift of the location of the maximum flow towards smaller densities.[10]
The simulation displays visible areas of zero and high density, similar to stop and go waves which can be observed in real traffic, for values of γ small compared to 1. This occurs for all three test average densities, 25%, 50% and 75%. For $\gamma = 1$, the pattern is always largely homogeneous, and the striped pattern cannot be reproduced for any values of density, α or β, so this simulation always mimics free flow traffic. As α is reduced, the lines of phase separation become sloped, so that as time advances, the discrete areas of maximum and minimum density move backwards in space, as in figure 2. This is a feature of stop and go waves in real traffic.
The influence of varying β, with α and γ set to small values, is minimal: the width of the lines of phase separation increase slightly.

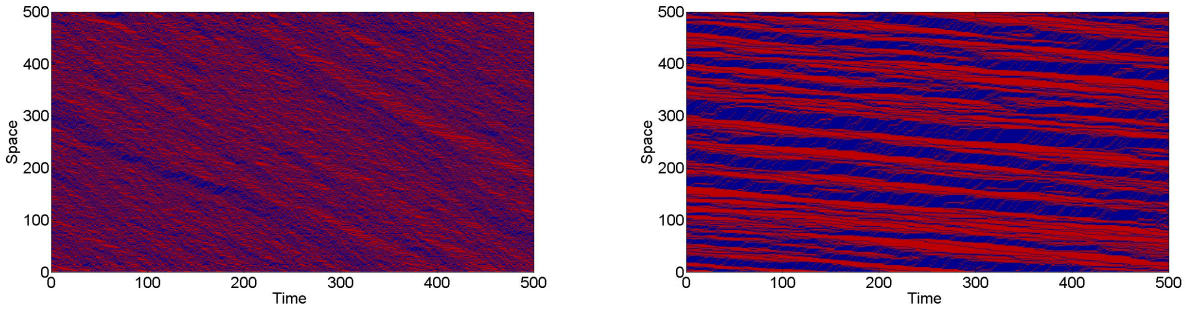

Figure 2: Stationary Traffic Patterns.
(Left) For $\gamma = 1$, no values of the density or the remaining parameters yield striped output. $\alpha = \beta = 0.1,\ \gamma = 1$ shown here.
(Right) For small values of γ the bands of occupied sites and unoccupied sites appear sloped, similar to stop and go waves in real traffic moving backwards in space as time advances. $\alpha = \beta = \gamma = 0.1$ shown here.

In order to establish if stop and go waves have a typical size, their spatial correlation and power spectrum were calculated. This was repeated for three densities, 25%, 50%, and 75%, for system sizes 1000, 500, 250, and 100, and for three sets of parameter values: $\alpha = \gamma = 0.1, \beta = 0.5$; $\alpha = \beta = \gamma = 1$; and $\alpha = \gamma = \frac{1}{19}$. This last case is the KLS model [11] for which the exact fundamental diagram can be calculated with periodic boundary conditions. In terms of the jump rates given above, $1 = 1 + \delta$, $\alpha = 1 - \delta$, $\beta = 1 - \epsilon$, $\gamma = 1 + \epsilon$ with $\delta = \epsilon = 0.9$. These identified only short short-range, correlations, and the M42 Data was used to verify that this is a physical reality.

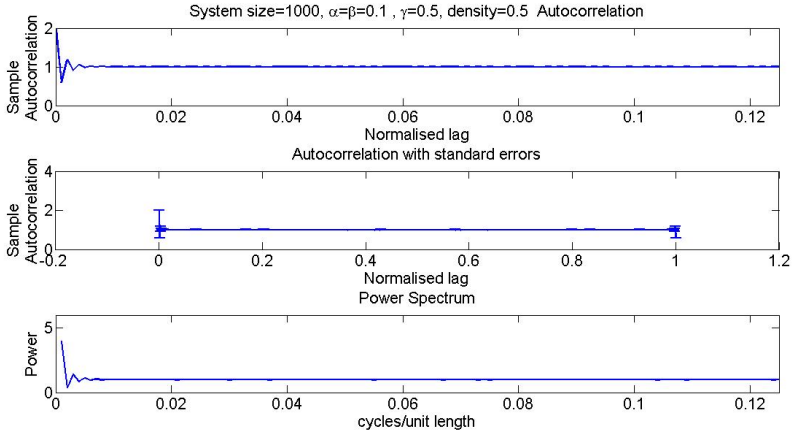

Figure 3: The spatial autocorrelation confirmed that there is no typical size for a jam in the simulations. As in the M42 Data, jams, including stop and go waves, exist in all sizes. See also figure 12

The autocorrelation was calculated for configurations $\eta(x)$, lattice size, L and lags k as follows:

$$\frac{1}{L}\sum_{k}\frac{\eta(x)\eta(x+k \; mod \; L)}{\rho(1-\rho)} \tag{12}$$

The power spectrum is the Fourier transform of the autocorrelation, and the normalised lag sets the maximum lag to 1.

3.2. The Single Bump

A single traffic jam was simulated to determine whether an initial condition of pre-existing jam influences the formation of stop and go waves, and illustrate the standard construction of entropy solutions following [5]. This, called the bump scenario in Gasser's paper [9], was simulated with an initial area of maximum density that was spatially fixed and varied in size, and simulations were run with the background densities 25%, 50% and 75% as before. The simulation was run 100 times and the average taken, as shown in figure 4. As the simulation runs diffusion is seen. As the traffic begins to move, the front interface of the jam (high density region) remains sharp, and moves backward in space. The periodic boundary conditions mean that there is traffic joining the back of the queue, which makes this interface more diffuse, although it moves rapidly through the density range, and may be considered to be relatively sharp on this scale. The parameter values were found to have the same roles as without an initial jam: stop and go wave-like output depends principally on the value of γ. There were no distinct areas of maximum and minimum density observed in the bump simulation, which were not also observed without this initial condition.
The characteristics of the PDE for this type of initial conditions, moving from maximum to zero density, spread out fan-like and this is a rarefaction. For $\gamma = 0.15$ both interfaces remain sharp on this scale, and this was used later to initialise simulation of stop and go waves.

The mode of diffusion was examined by taking density profiles at time intervals in the simulation (figure 5). These show that the accelerating (exit) interface tends to remain sharp, and diffusion occurs at the decelerating, (arrival) interface. It also highlights that the sharp accelerating interface moves backwards in space as time moves forward. The density profiles computed for this scenario accord with the entropy conditions and Fundamental Diagram construction

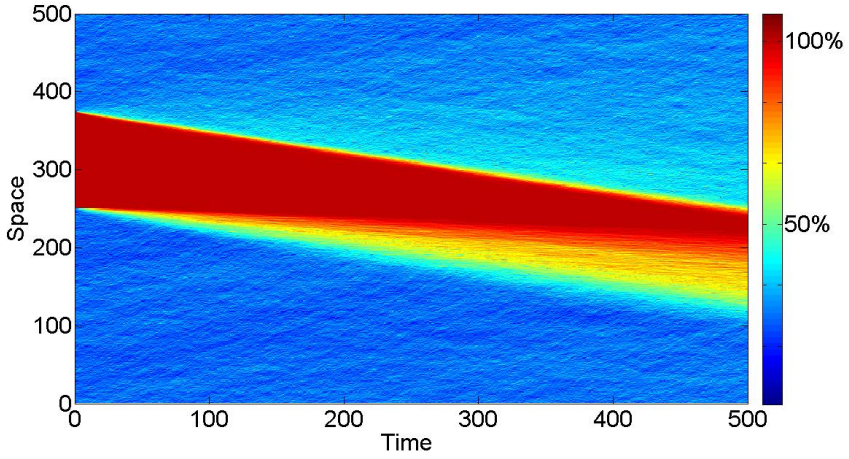

Figure 4: Traffic density time evolution of a jam.
For parameters$\alpha = \beta = 0.1$, $\gamma = 0.5$, this simulation is of the bump scenario where there is an initial spatially fixed patch of maximum density traffic. This simulation ran with a background density of 25% elsewhere. Average density over 100 realisation with lattice size 500 and 500 timesteps, and periodic boundary conditions. Initial jam is set to 25% of lattice size with zero density on 10% of lattice immediately ahead of jam.

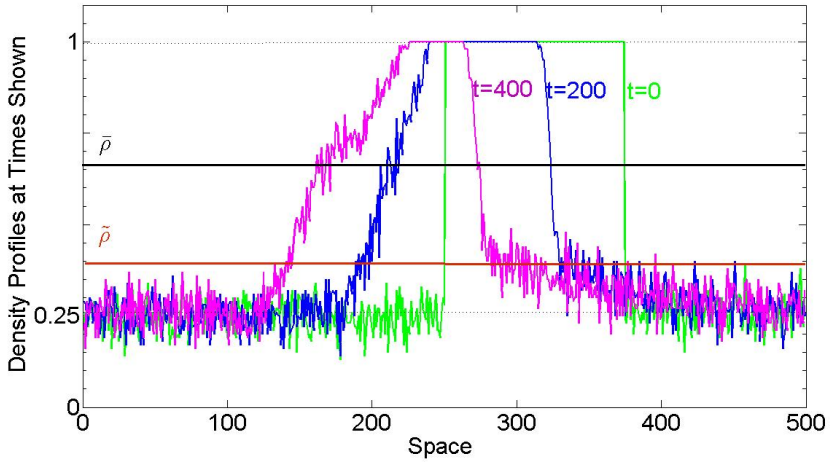

Figure 5: Snapshots of the density profile at start, mid and end times, average of 100 simulation runs .
The area of high density moves backward in space, and the accelerating interface remains sharp whilst the decelerating interface is dissolving. The locations of $\bar{\rho}$ and $\tilde{\rho}$ are marked at the values given by the Fundamental Diagram for the same parameters, see figure 6. For $\rho_L < \rho_R$, the decelerating interface, there is a change of slope at $\bar{\rho}$ and times t=250 and t=500, where the change from shock to rarefaction is predicted. For $\rho_R > \rho_L$, the accelerating interface, there is a change of slope at $\tilde{\rho}$ and times t=250 and t=500, where the change from rarefaction to shock is predicted.

described in Gasser [9] see figure 6. The secant between the value of $j(\rho)$ at the background density, 0.25, and the tangent at the point where $j(\rho)$ changes from strictly concave to strictly convex forms the lower convex envelope. The value of ρ at which this change occurs is marked $\bar{\rho}$. For the decelerating (arrival) interface, the condition $\rho_L < \rho_R$ exists, and standard PDE theory predicts a change will occur from shock to rarefaction. This value of ρ on the density profiles coincides with a change of slope, which is more pronounced for the later times. The secant between $\rho_{max} = 1$ and the tangent with $j(\rho)$ forms the upper convex envelope.
The value of ρ at which this tangent occurs, is marked $\tilde{\rho}$. For the accelerating (exit) interface, the condition $\rho_L > \rho_R$ exists, and standard PDE theory predicts a change will occur from rarefaction to shock. As previously, this value of ρ on the density profiles, a change of slope is observed, which is less pronounced for later times.

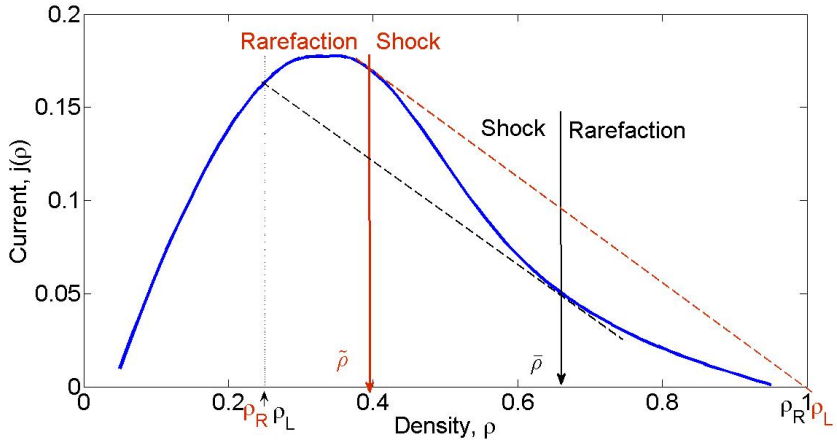

Figure 6: Fundamental Diagram for the bump scenario with 0.25 background density and $\alpha = \beta = 0.1$ and $\gamma = 0.5$.
The situation for the decelerating interface, where $\rho_L < \rho_R$, is shown in black and the change of behaviour from shock to rarefaction is predicted to occur at $\bar{\rho}$ For the accelerating interface, the text is in red, and the change from rarefaction to shock is predicted at $\tilde{\rho}$.

This simulations result shows that the corresponding Lighthill, Whitham and Richards model describes the cellular automata on a large scale correctly with standard entropy solutions. Since both models were derived from different viewpoints, this result is partly unexpected.

4. Comparison with Real Data

4.1. M42 Data

The Highways Agency employs Intelligent Transport Systems in which Information and Communication Technologies are used to manage traffic in order to alleviate traffic congestion, which costs UK businesses up to £20 billion annually. Active Traffic Management (hard shoulder running on Birmingham's M42 motorway) is the latest of these schemes which activate automatically at peak times in an attempt to stabilise flow and so reduce congestion and accidents [3].

Four samples from the M42 Active Traffic Management data collection were chosen on the basis that they displayed interesting behaviour such as stop and go waves, jams, and congested merges, and these were used to improve and inform the Markov model, e.g. in the selection of parameter values. (See figure 7) A stop and go wave is a structure which propagates upstream against the flow of traffic and has two sharp interfaces, one at which vehicles brake, and one at which they accelerate, bounding a plateau of slow-moving traffic [3]. A congested merge is a particular kind of traffic jam which builds up behind the on-flow of a slip road.

The M42 has a uniquely high coverage of inductance loop detectors, between junctions 3a and 7, a stretch of approximately 11 miles. Single loop detectors measure only flow and lane occupancy, and double loop detectors also measure vehicles' velocities and lengths [4]. The data consist of 24 hours' readings of flow and speed from 183 induction loop detectors along a 16km stretch of the motorway. Both measurements are pre-processed into one-minute averages and rounded to integer values. The spacing of the loops is nominally 100m along the majority of this stretch, with a small subsection where spacing is nominally 30m. The dataset includes a vector of nominal spacing, which was used to further process the output into more evenly spaced readings. The true spacings are known to vary slightly, but exact distances are not yet available and are not relevant for our purpose.

The data is visualised as a colormap, with the colour indicating the values of speed and flow respectively. The slow moving, low flow traffic can be seen in red, and the almost vertical stripes indicate jams and stop and go waves. The horisontal lines indicate faulty induction loop detectors. The data for February 5th shows two sets of stop and go waves, one in the morning rush hour and one in the evening. The morning rush hour, between 450 minutes(7.30am) and 630 minutes (10.30am), originated at the congested merge around 6km, and the evening rush hour, between 3.30pm and 7pm, at the congested merge around 14km. The data for the 1st August shows a particularly large set

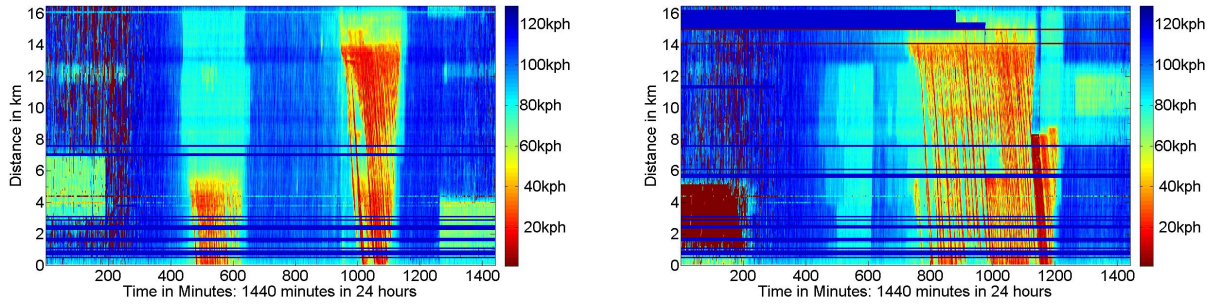

Figure 7: Speed: Left is M42 data for 5th February 2008, Right is 1st August 2008
Speed is indicated by colour. Notice the almost vertical red stripes indicating jams and stop and go waves. Horizontal stripes are caused by faulty detectors.

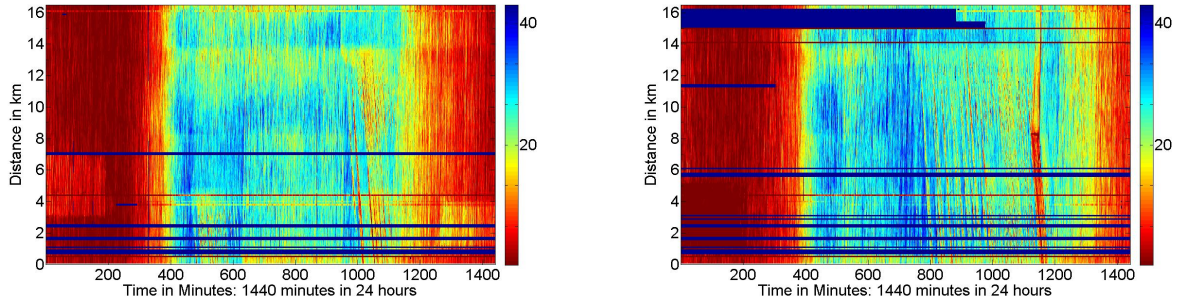

Figure 8: Flow: Left is M42 data for 5th February 2008, Right is 1st August 2008
Flow is indicated by colour, and is measured in vehicles per minute. As for speed readings, the almost vertical red stripes indicate jams and stop and go waves, and horizontal stripes are caused by faulty detectors.

of stop and go waves beginning around midday and lasting until 8pm. There is also a bigger, more persistent jam beginning around 8km at 6.45pm and remaining static for a full 30 minutes at the point of origin. It began to clear, broke into stop and go waves, and finally resolved at 8.10pm.

4.2. Fundamental Diagrams

The Fundamental Diagram is the flux function, and for different parameter values, the simulation flux function is either concave or neither convex nor concave.
For $\alpha = \beta = \gamma = 0.1$ the simulation Fundamental Diagram is strictly concave. For the same values of α and β, and γ greater than 0.15, the Fundamental Diagram is neither concave nor convex, as in figure 6. For these parameter values, the simulation does not produce striped output. The simulation successfully reproduces the KLS Fundamental Diagram.
The Fundamental Diagram for the M42 Data is neither concave nor convex in the flux / density form. In traffic literature, the Fundamental Diagram is sometimes approximated by the flow / velocity, and in this case, it is strictly concave.

The Fundamental Diagrams for the M42 data show a smooth curve where it is strictly increasing, with greater variation when it begins to decrease. It was also discovered that for some fixed speeds, all to the right of the Fundamental Diagram's maximum, the flow distribution switches from unimodal to bimodal and back. This is supported as a general result: in [3] states that large fluctuations are found in empirical data to the right of the fundamental diagram's maximum.The flow / speed diagram, figure 9, is strictly concave for all four sample days. The flow / density diagram, figure 9, is neither concave nor convex. The density was estimated by flow/speed and the plot show artifacts such as asymptotes caused by the use of averaged, rounded data in both denominator and numerator. In addition, the bins used to calculate the mean flow value included the lower boundary but not the upper boundary of the bins, so that

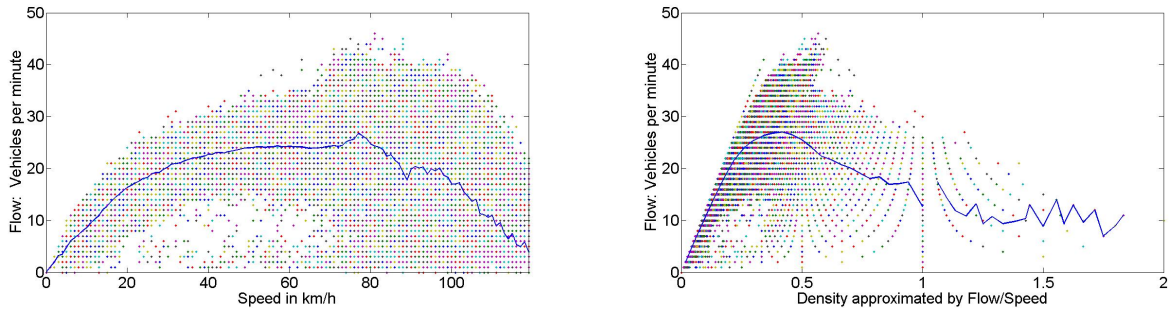

Figure 9: (Left) M42 Data 11th January 2008: Flow data and mean flow & speed
In the literature the Flow/Speed diagram is sometimes used to approximate the Fundamental Diagram. The line is the mean flow and the colours of the data points are not significant. (Right) M42 Data 11th January 2008: Flow data and mean flow Fundamental Diagram
The Fundamental Diagram is not strictly concave.
The asymptotes are numerical artifacts due to small number of integer data points. The line is the mean flow and is highly variable for Flow/Speed> 1 as a result of few data points here. The colours of the data points are not significant.

the over-representation of 1 resulted in a spike in the average value, just after density=1, for each of the days sampled. The simulation Fundamental Diagram was produced for several sets of test parameter values including: the pure slow to start scenario, $\alpha = \gamma = 0.1$, $\beta = 1$, the only look ahead scenario, $\alpha = \beta = 0.5$, $\gamma = 1$, and $\alpha = \beta = 0.4$, $\gamma = 0.7$. The comparison with the mean of the 4 samples' flow / speed diagrams reveals the fits.

The induction loop detectors are in place, not principally to provide data for scientific study, but for the active traffic management. There is data available to indicate when the active traffic management is in force, and when it is not, but we did not have access to that information. It may explain the bimodality of the flow distributions for the flow / velocity diagram.

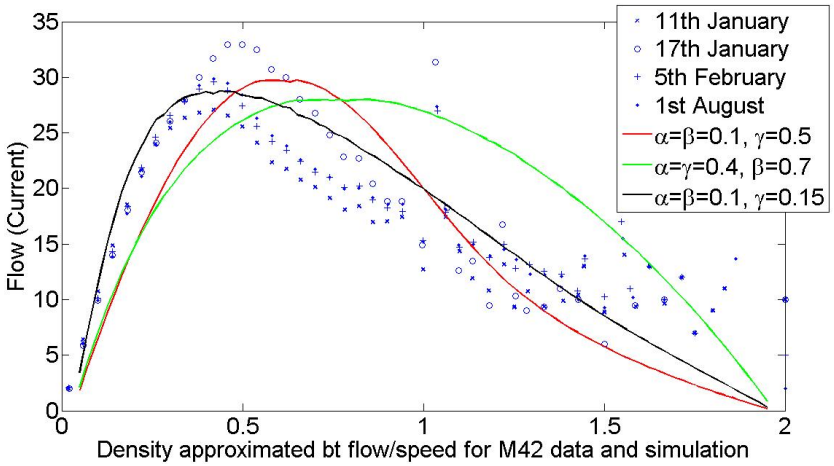

Figure 10: The Fundamental Diagram of the M42 and simulation.
There are no other parameter values that give a better fit, but this correspondence is not entirely satisfactory

There may be parameter values which give a better fit but these become non-physical in terms of real traffic. (Some classes of models can produce backward flowing traffic!) [3].

The simulations run with parameter values which have a reasonable physical interpretation are able to produce Fundamental Diagrams which are a fairly good fit with the samples of real world observations. It is not obvious that this should be the case for such a simple cellular automaton model.

4.3. Stop and Go Waves

A stop and go wave is a structure which propagates upstream against the flow of traffic and has two sharp interfaces, one at which vehicles brake, and one at which they accelerate, bounding a plateau of slow-moving traffic [3].
The speed profiles from the M42 data, taken at a fixed time over all locations shows there is no typical size for the stop and go waves (cf figures 2 3, and the flow profiles suggest that the exit speed does not vary significantly. Plotting successive minute averages gives an idea of the variation. The position of the curves can be seen moving backwards in space for stop and go waves and remaining fixed in space for congested merges.

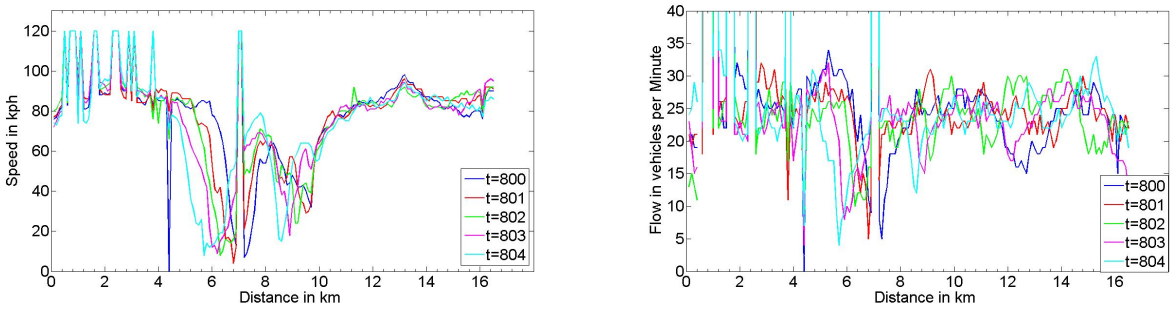

Figure 11: M42 data 11th January 2008 Speed and flow plotted at successive minutes.
(Left) Speed: The minimum speed is shown to move backwards in space, and the speed is shown to be more variable in the jam than in free flow. This wave is 5km long. The sudden peaks at 120kph are faulty detectors.
(Right) Flow: The flow minima also move backwards in space but the variation is constant throughout the traffic patterns. As above, the readings in excess of 40 vehicles per minute are faulty detectors.

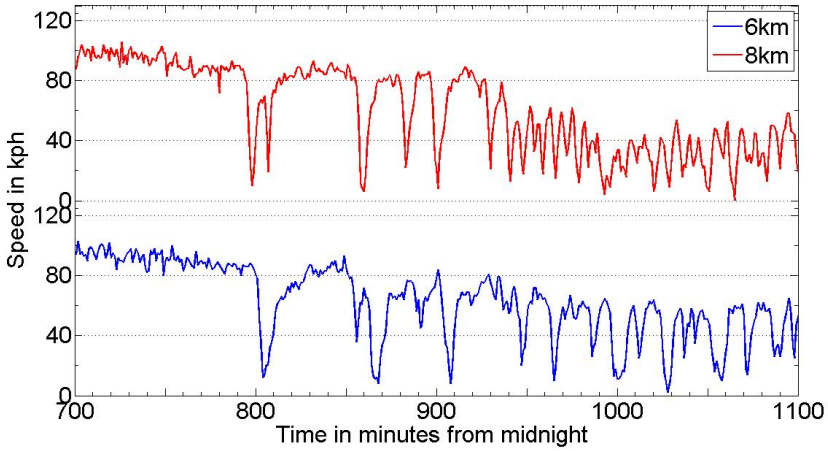

Figure 12: Speed plotted at two different locations across a section of stop and go waves shows there is no typical spatial size for a stop and go wave in this data, as in the simulation.

Stop and go waves were simulated using the parameter set $\alpha = \beta = 0.1$, $\gamma = 0.15$. Each lattice site was used to represent approximately 6m and a timestep to represent 1 second, the simulation was run for a lattice size of 2500 and periodic boundary conditions (representing 15km) and 50,000 timesteps (representing 3 hours). This was compared to a 3-hour window on 11th January. There are both clear similarities and differences evident here. The simulations stop and go waves to not maintain their integrity on physical time scales, dissolving in relatively short times, and the periodic boundary conditions are clearly not representative of physical reality. Nevertheless, the slope of the waves, which is the slope of the high density section of the Fundamental Diagram, faithfully reproduces the slope of the stop and go waves seen in the real data. In addition, the simulation stop and go waves were shown to have no typical spatial

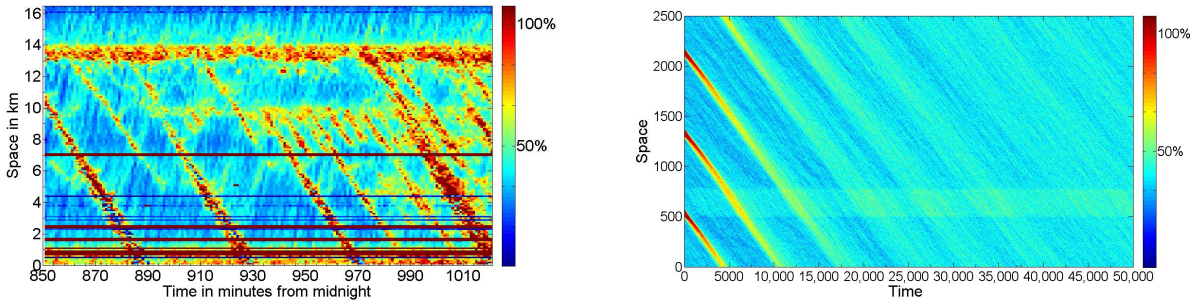

Figure 13: Stop and go waves: M42 data and Simulation
(Left) A 3-hour window of the M42 data from 11th January 2008 shows the structure of the stop and go waves. The horisontal stripes e.g. at approx 7km, are faulty detectors which always read maximum or minimum density. The poor resolution is the result of approximating density by flow/speed, both of which are minute averages rounded to integers.
(Right) The simulated stop and go waves on a similar time and space scale all diffuse whilst in real traffic some dissolve but others are stable, and may grow in width. The periodic boundary conditions are clearly visible here.

size, also corresponding to the physical reality as seen in M42 data. refer to earlier discussion in 3.2.

Although the replication is far from perfect, it is surprising that the stop and go waves, produced with such a simple microscopic model, have a significant degree of correspondence with observed real data.

5. Conclusions

The goal of this study was to further the understanding of traffic flow described on different scales, through the examination of the macroscopic Lighthill, Witham and Richards conservation law description and a cellular automata microscopic model.

The simulation example of the bump was analysed by examining density profiles at representative intervals. This revealed that the behaviour of the simulation was the behaviour predicted by the Lighthill, Whitham and Richards PDE model with standard entropy conditions.
The conclusion drawn is that the connection between the microscopic and macroscopic descriptions of traffic have been shown to exist through the Fundamental Diagram. The macroscopic model is, somewhat unexpectedly, able to describe correctly the microscopic model on large scale without the need to derive some new entropy solutions.

The simulation uses only local information whilst drivers in real traffic base their decisions on increased information derived from observations further ahead and behind.
Nevertheless the conclusion can be drawn that thee microscopic model is able to connect with real data, despite its simplicity, in producing Fundamental Diagrams which are a fairly good fit using parameter values which have a reasonable physical interpretation.

Stop and go waves are a feature of particular interest, since in real traffic they are a cause of so much wasted resources. A successful model of these would pave the way to their reduction and perhaps elimination.
This simple microscopic model is capable of producing stop and go wave behaviour which corresponds to the physical system in important ways.

Future work may include investigation into the stability of simulated stop and go waves on physical scales. This is known to be hard, as it usually leads into parts of the model parameter space which produce non-physical traffic behaviour [3].
The discovery of a functional form for the Fundamental Diagrams produced by the simulations or by real data could be connected to the macroscopic description via examination of the function's characteristics.

Acknowledgments

The support of my supervisor, Dr Stefan W. Grosskinsky, whose encouragement, guidance and enthusiasm enabled me to develop an understanding of the subject is acknowledged with much gratitude.
Dr. R. Eddie Wilson, from the Univeristy of Bristol, gave us the benefit of his considerable experience in handling real traffic data, and his invaluable support is acknowledged with thanks.
This work was funded by EPSRC through the Warwick Complexity Science Doctoral Training Centre

References

[1] Lighthill, M.J and Whitham, G.B (1955) A theory of traffic flow on long, crowded roads Proc. R, Soc. A 229, 317-345
[2] Piccoli, B. and Garavello, M. (2006) *Traffic Flow on Networks* USA: American Institute of Mathematical Sciences.
[3] Wilson, R.E. (2008)Mechanisms for spatiotemporal pattern formation in highway traffic models
[4] Wilson, R.E. (2008)'From Inductance Loops to Vehicle Trajectories' Submitted to the TRB annual meeting.
[5] Lax, P.D.(2006)*Hyperbolic Partial Differential Equations*. USA: American Mathematical Society
[6] Fowkes, N.D and Mahony, J.J. (1996) *An Introduction to Mathematical Modelling* Sussex: John Wiley & Sons.
[7] Knowles, J.K.(2008) 'On entropy conditions and traffic flow models' Math. Mech. 88, No.1, 64-73.
[8] Ansorge, R. (1990) 'What does the entropy condition mean in traffic flow theory?' Transpn. Res.-B Vol 24B, No.2. pp133-143
[9] Gasser, I. (2003) Short Communication on non-entropy solutions of scalar conservation laws for traffic flow Math. Mech. 83, No.2, 137-143 Knowles, J.K. (2008)On entropy conditions and traffic flow models Math. Mech. 88, No.1, 64-73.
[10] Schadschneider, A. and Schreckenberg, M. (1997)'Traffic flow models with 'slow-to-start rules' arXiv:cond-mat/9709131v1 [cond-mat.stat-mech]
[11] Grosskinsky, S. (2004) 'Phase transitions in nonequilibrium stochastic particle systems with local conservation laws' PhD thesis see www.warwick.ac.uk/ masgav/ under publications.
[12] Dafermos, C.M. (2000) *Hyperbolics Conservation Laws in Continuum Physics* Berlin: Springer
[13] S. Katz, J.L. Lebowitz, and H. Spohn.(1984) 'Nonequilibrium steady states of stochastic lattice gas models of fast ionic conductors.' J. Stat. Phys. 34(3/4): 497537.